Geophysical Research Letters

RESEARCH LETTER
10.1029/2021GL097402

Key Points:

- Steady-state schemes allow users to control the nuclear magnetic resonance (NMR) signal's location in the spectra
- Steady-state schemes can be exploited to increase separation between the NMR signal and nearby narrow-band noise sources
- Frequency shifted steady-state surface NMR data can be inverted reliably

Correspondence to:

D. Grombacher,
denys.grombacher@geo.au.dk

Citation:

Grombacher, D., Griffiths, M. P., Liu, L., Vang, M. Ø., & Larsen, J. J. (2022). Frequency shifting steady-state surface NMR signals to avoid problematic narrowband-noise sources. *Geophysical Research Letters*, *49*, e2021GL097402. https://doi.org/10.1029/2021GL097402

Received 8 DEC 2021
Accepted 14 MAR 2022

Frequency Shifting Steady-State Surface NMR Signals to Avoid Problematic Narrowband-Noise Sources

D. Grombacher[1,2], M. P. Griffiths[2,3], L. Liu[1,2], M. Ø. Vang[1,2], and J. J. Larsen[2,3]

[1]Hydrogeophysics Group, Department of Geoscience, Aarhus University, Aarhus, Denmark, [2]Aarhus Center for Water Technology, Aarhus University, Aarhus, Denmark, [3]Department of Electrical and Computer Engineering, Aarhus University, Aarhus, Denmark

Abstract Recent developments in surface nuclear magnetic resonance (NMR) based on steady-state sequences show great enhancements in signal quality and mapping speeds. We demonstrate how manipulating the timing and phase of these sequences can shift the NMR signal away from problematic narrow-band noise sources, for example, co-frequency powerline harmonics, or shift narrowband noise sources away from the NMR signal. The spectral separation of the NMR signal from co-frequency noise sources enables production of high-quality data under one of the most challenging noise scenarios in surface NMR. We demonstrate the feasibility with surface NMR measurements at a site where the Larmor frequency coincides with a powerline harmonic. We separate the NMR signal and powerline noise by up to 5 Hz and obtain high-quality data, which are readily inverted. The approach is straightforward to implement, well suited for field processing, and shows great potential to expand the range of conditions allowing surface NMR measurements.

Plain Language Summary The surface nuclear magnetic resonance (NMR) signal can be difficult to isolate in the presence of a high-amplitude noise source with an overlapping frequency, such as when a strong powerline harmonic sits atop the NMR signal. We demonstrate that the timing of surface NMR steady-state sequences can be manipulated to alter the location of the NMR signal in the frequency domain, allowing one to separate the NMR signal from the overlapping strong noise source. Field results are given highlighting the feasibility of the technique and demonstrating that high fidelity NMR signals can be extracted even when they share a frequency with a higher amplitude powerline harmonic.

1. Introduction

Surface nuclear magnetic resonance (NMR) provides direct sensitivity to water content at depth (Weichman et al., 2000), offering profiling of water abundance (Legchenko & Valla, 2002) and insights into pore-scale conditions (Kenyon et al., 1988; Mohnke & Yaramanci, 2008). A chief difficulty in surface NMR is dealing with high-energy narrow-band noise sources appearing close to the NMR signal in the frequency domain (Liu et al., 2017). Powerline harmonics are the most commonly encountered noise source of this type, where 50 or 60 Hz harmonics are often present with significantly more energy than the NMR signal in the frequency band of interest. Generally, powerline harmonics can be robustly mitigated using a variety of approaches (Larsen et al., 2014), but these schemes often struggle in the limit where a harmonic exists within several Hz of the NMR signal (Wang et al., 2018)—a condition commonly referred to as a co-frequency harmonic in the surface NMR literature. Several processing workflows have been explicitly tailored to address co-frequency issues, focused on either modeling and removing this signal (Liu et al., 2017; Wang et al., 2018) or on exploiting spectral properties of data windows (Grombacher, Kass, et al., 2020; Grombacher, Liu, et al., 2020). Each of these schemes have been developed in the context of free-induction decay (FID) acquisition strategies and focus on denoising the time-domain NMR signal.

In this work we focus on a recently developed steady-state approach to surface NMR acquisition, where the NMR signal is collected during a train of identical pulses each separated by a fixed delay time (Carr, 1958; Grombacher et al., 2021). This approach has been demonstrated to offer significant signal-to-noise ratio enhancements over traditional FID approaches. Of particular interest is the ability of steady-state processing schemes to collapse the surface NMR signal into an extremely narrow frequency band. The advantage being that the relevant noise bandwidth contributing to the effective signal-to-noise ratio of the signal is reduced compared to traditional workflows; from several hundred Hz to <1 Hz. A feature of the steady-state processing workflow is that the

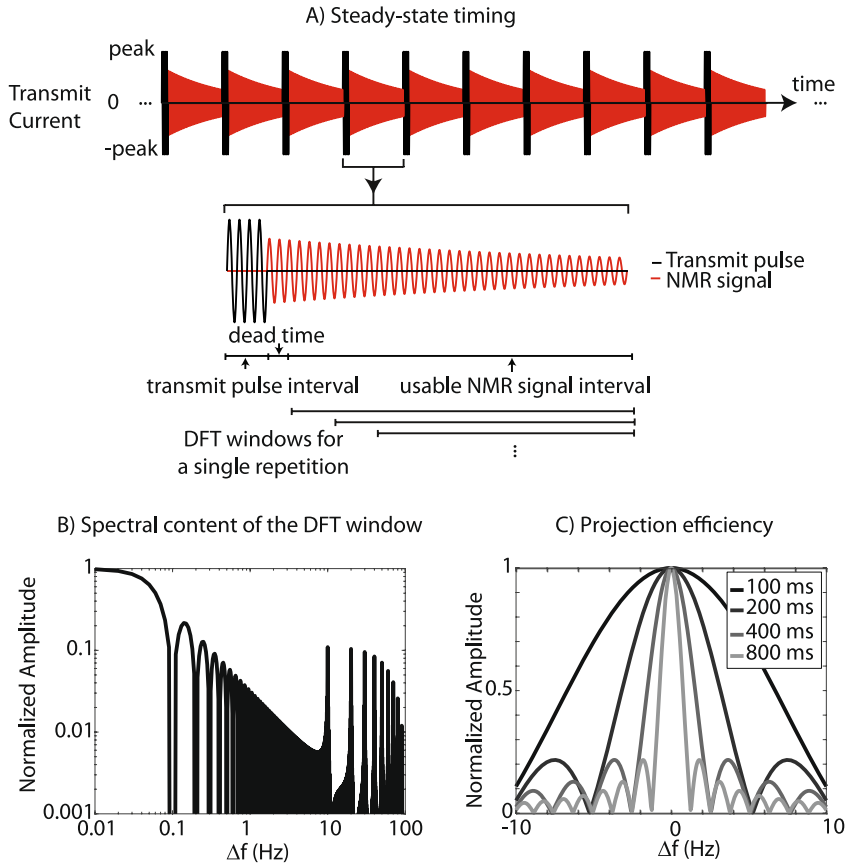

Figure 1. (a) Timing of the steady-state sequence. (b) The spectral content of a window corresponding to a 60 s duration steady-state sequence with a 10 ms pulse, a 100 ms repetition time and transmit frequency of 2,150 Hz. (c) The projection efficiency for a range of ω_j–ω_0 offsets for four repetition times (colors correspond to tend).

location of the NMR signal in the spectra is controlled by the timing of steady-state pulse train. That is, the NMR signal will be localized at harmonics of the pulse repetition frequency (the inverse of t_{rep}, the time interval between pulses), appearing not necessarily at the Larmor frequency but at a frequency defined by the steady-state sequence. We show that this feature can be exploited to manipulate the location of the NMR signal in the spectra, or to manipulate the location of problematic noise sources. We present a field example where the NMR signal has been isolated from an overlapping powerline harmonic and demonstrate the ability to reliably invert data where the NMR signal's location has been manipulated.

2. Background

Surface NMR measurements involve perturbing a magnetization at depth that originates from the immersion of hydrogen nuclei in Earth's magnetic field (Hertrich, 2008). The magnitude and time-dependence of this magnetization provides insights into water abundance and pore-scale properties. To image spatial variability of water content and of relaxation times controlling the magnetizations' time-dependence a sounding approach is used, where NMR signals are measured following a suite of excitation pulses of various strengths (Legchenko & Valla, 2002). Traditionally, most measurements employ a FID scheme, measuring the NMR signal produced by a single excitation pulse and then waiting several seconds prior to the subsequent measurement to ensure re-equilibration of nuclear spins.

An alternative measurement scheme involves measuring the NMR signal produced by a train of closely separated identical pulses, called a steady-state sequence (Carr, 1958, e.g., Figure 1a). The train of pulses drive the magnetization into a new equilibrium, the properties of which can be rapidly measured to produce a high-quality signal in a short period of time. The interval between pulses are significantly shorter than the wait times for FID

schemes, hundreds of milliseconds versus 2–5 s. Steady-state schemes can be deployed for sounding style acquisitions, where the steady-state data is measured for a range of current amplitudes, pulse durations and repetition times. The repetition time between neighboring pulses is selected to coincide with an integer number of periods of the transmit frequency. Tying the repetition time to the transmit frequency in this manner ensures subsequent pulses are either in-phase or out-of-phase (achieved by altering the pulse polarity). Steady-state data collected using different sequences is inverted jointly to produce depth profiles of water content, the effective transverse relaxation time T_2*, and the transverse relaxation time T_2. In contrast, traditional FID approaches generally only estimate water content and T_2*—the relaxation time with more ambiguous links to pore-scale properties of interest (Grunewald & Knight, 2011).

Surface NMR steady-state processing schemes involve a multi-windowing scheme where the discrete Fourier transform (DFT) of the entire time-series is taken, but with the pulsing intervals and selected intervals of the NMR signal zeroed, Figure 1a. The output of this scheme is N_{seg} DFT values for different windowed versions of the same underlying time-series. The reasoning for the multi-windowing approach is to weight different portions of the record, that is, times immediately after the pulse or times significantly after the pulse, differently to encode additional relaxation time information into the data set. Note that the data and modeling are both in the frequency-domain—forming the "decay" is simply a convenient data-visualization tool. Figure 1b show the spectral content of a 60 s long DFT with 10 ms windows zeroed out every 100 ms. The <1 Hz main lobe highlights that the noise bandwidth contributing to the processed data is extremely narrow.

It is common that NMR signals have bandwidths exceeding 10 Hz, that is, much wider than the main lobe of the DFT. However, the narrow DFT bandwidth still captures the full bandwidth of the NMR signal. We show this by computing the projection efficiency, which measures the contribution from off-resonance components to the DFT value. Consider the DFT integration across a single window with an example NMR signal, $s(t)e^{i\omega_0 t}$ with amplitude $s(t)$. For simplicity we use complex notation and focus only on the component oscillating at ω_0. The integration occurs from a time t_{st} until t_{end} after the pulse, and the DFT is performed at ω_j.

$$S(\omega_j)_1 = \int_{t_{st}}^{t_{end}} s(t)e^{i\omega_0 t}e^{-i\omega_j t}dt \tag{1}$$

here $S(\omega_j)_1$ is the single window contribution to the DFT taken at ω_j for the ω_0 NMR signal component. For a simplified scenario where $s(t) = 1$ (*i.e.*, a flat envelope over the window), only the complex exponential terms are left in Equation 1. Figure 1c illustrates the solution to Equation 1 for a range of ω_j–ω_0 offsets for four different t_{end}. In each case, t_{st} is equal to 10 ms.

The projection efficiency curves in Figure 1c have significantly less attenuation with frequency offset than the spectral content in Figure 1b. The reason for this is that the projection efficiency is based on a single window—a significantly reduced interval compared to the 60 s window used to form the plot in Figure 1b. This is a consequence of the fact that the signal is repeating every segment while the noise is not. Of importance is that the ambient noise contribution to the steady-state signal is attenuated based on the spectral content in Figure 1b, while off-resonance NMR components attenuation is instead dependent on Figure 1c.

Equation 1 considers the contribution to the DFT at ω_j of the ω_0 component across a single window. The DFT for a full duration signal is given by,

$$S(\omega_j) = \int_0^{t_{max}} s(t)e^{i\omega_0 t}w(t)e^{-i\omega_j t}dt \tag{2}$$

where t_{max} is the duration of the measurement, for example, 60 s, and $w(t)$ is the window function that zeroes the pulse affected intervals. Equation 2 can be rewritten as the sum of N individual windows,

$$S(\omega_j) = \sum_{k=1}^{N} \int_{t_{st,k}}^{t_{end,k}} s(t)e^{i\omega_0 t}e^{-i\omega_j t}dt \tag{3}$$

here $t_{st,k}$ and $t_{end,k}$ represent the start and end time of the *kth* window, respectively. The signal $s(t)$ is identical in every window, a consequence of the NMR system being in a steady-state. Equation 1 describes the first window in this sum, while the *kth* window is given by

$$S(\omega_j)_k = \int_{t_{st}+(k-1)*t_{rep}}^{t_{end}+(k-1)*t_{rep}} s(t) e^{i\omega_0 t} e^{-i\omega_j t} dt \quad (4)$$

The integration limits in Equation 4 are shifted by an integer number of repetition times t_{rep} compared to the first window (Equation 1). This allows Equation 4 to be rewritten through a change of variables ($t' = t - (k-1)*t_{rep}$) as,

$$S(\omega_j)_k = e^{-i\omega_j(k-1)t_{rep}} \int_{t_{st}}^{t_{end}} s(t') e^{i\omega_0 t'} e^{-i\omega_j t'} dt' = e^{-i\omega_j(k-1)t_{rep}} S(\omega_j)_1 \quad (5)$$

From Equation 5 we see that the contribution from the k'th window to $S(\omega_j)$ is simply the first window's contribution multiplied by a phase factor. We can therefore recast Equation 2 as

$$S(\omega_j) = \left(\sum_{k=1}^{N} e^{-i(k-1)\omega_j t_{rep}} \right) S(\omega_j)_1 = e^{-i\omega_j t_{rep}(N-1)} \frac{\sin(\omega_j t_{rep} N/2)}{\sin(\omega_j t_{rep}/2)} S(\omega_j)_1 \quad (6)$$

The factor preceding $S(\omega_j)_1$ is the Dirichlet or periodic sinc function. This is a comb-like function with peaks appearing at integer multiples of $1/t_{rep}$. This term is responsible for the collapse of the steady-state spectrum into extremely narrow peaks in the frequency domain.

Of interest in this work is that the location of the peaks in the Dirichlet function are determined by $1/t_{rep}$; not ω_0. Note that t_{rep} is a user-defined parameter, giving the user freedom to select where in the spectra the NMR signal will appear. Traditionally, the NMR signal appears at ω_0, its intrinsic frequency, but the repetitive nature of the steady-state train and the resetting of the NMR signal phase following each pulse results in the NMR signal shifting its location in the frequency domain onto nearby harmonics of $1/t_{rep}$. We propose that this feature can be exploited to avoid problematic noise sources in the frequency domain—such as a narrow-band power line harmonic.

3. Results

Figure 2 shows spectra and sounding curves for data collected at a site near Sunds, Denmark where the local Larmor frequency was estimated to be 2,149.6 Hz using a magnetometer. This leaves only a 0.4 Hz separation from the anticipated location of the 2,150 Hz powerline harmonic. Note that the harmonics drift based on changes in the fundamental powerline frequency; for example, a ±50 mHz (as observed in Liu et al., 2017) shift in the fundamental frequency moves the 43rd harmonic approximately ±2.15 Hz away from 2,150 Hz in the spectra. Data was collected using the Apsu surface NMR system (Larsen et al., 2020), and a 50 by 50 m square coincident loop coil. Four data sets are illustrated in Figure 2. From left to right the sequences employed pulse repetition times corresponding to 200, 400, 800, and 200 periods of the transmit frequency. All sequences employed a 10 ms pulse, except for column 3, which used a 40 ms pulse. The three left-most columns correspond to "regular" steady-state sequences, where all pulses are in-phase. This represents the signal scenario described in Equation 6. Note the high amplitude noise source near 2,150 Hz in Figures 3a–3c, which corresponds to the 43rd powerline harmonic. The frequency of the harmonic shifts during and between measurements but is entirely overlapping the estimated Larmor frequency in Figures 3a–3c, shown by the red arrows. To deal with this, steady-state sequences that were deliberately transmitted at 5, 2.5, and 1.25 Hz off-resonance were performed. In each case, the repetition time is adjusted to ensure it contains an integer number of transmit periods—which corresponds to changes in the repetition time on the order of 10 s of microseconds. The location of the NMR peak in the spectrum is highlighted by the location of the blue arrows—coincident with the transmit frequency. In each case, the NMR peak has been shifted by a user-defined distance (highlighted by the black lines) away from its original location in order to increase separation from the problematic powerline harmonic. Figures 3e–3g show the sounding curves associated with each steady-state sequence for different peak current amplitudes. The circled point in the sounding curve corresponds to the spectra in the upper row. These spectra are chosen to span a range of peak currents, and are representative of the other measurements. Taken together, the sounding curves in 3E-G and the spectra in 3A-C demonstrate that high-quality data can be collected in the presence of an overlapping high-amplitude powerline harmonic with significantly more energy than the NMR signal. The relative energy between the

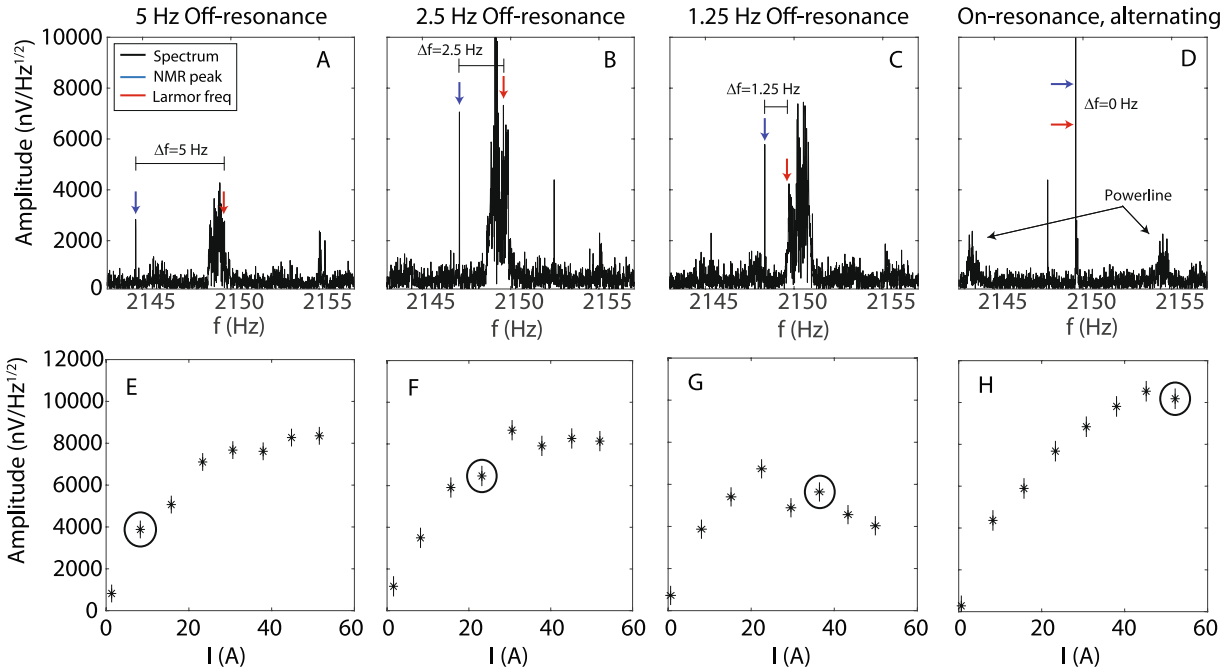

Figure 2. (a–d) Illustrate spectra corresponding to the circled data points in the sounding curves illustrated in (e–h). Each column corresponds to a particular steady-state sequence and offset.

NMR signal and powerline harmonic would likely make it extremely difficult to recover a high-quality signal or outright prohibit standard measurements under these conditions.

The rightmost column in Figure 2 corresponds to a steady-state sequence referred to as "alternating," which means that subsequent pulses have alternating polarity. In this case, an additional step in the processing is required—as the NMR signal produced by the positive and negative polarity pulses in the train are $s(t)$ and $-s(t)$, respectively. That is, they produce identical signals but of opposite sign. To remove this alternating signal polarity—even windows are multiplied by -1 to produce a signal described by Equation 3. The windowing and DFT steps can then proceed as normal, producing an NMR signal that appears at harmonics of $1/t_{rep}$ in the spectra. However, for any signal that does not switch polarity between neighboring pulses—that is, any signal that is not the steady-state NMR signal, such as a powerline harmonic—multiplying even windows by -1 is equivalent to multiplying

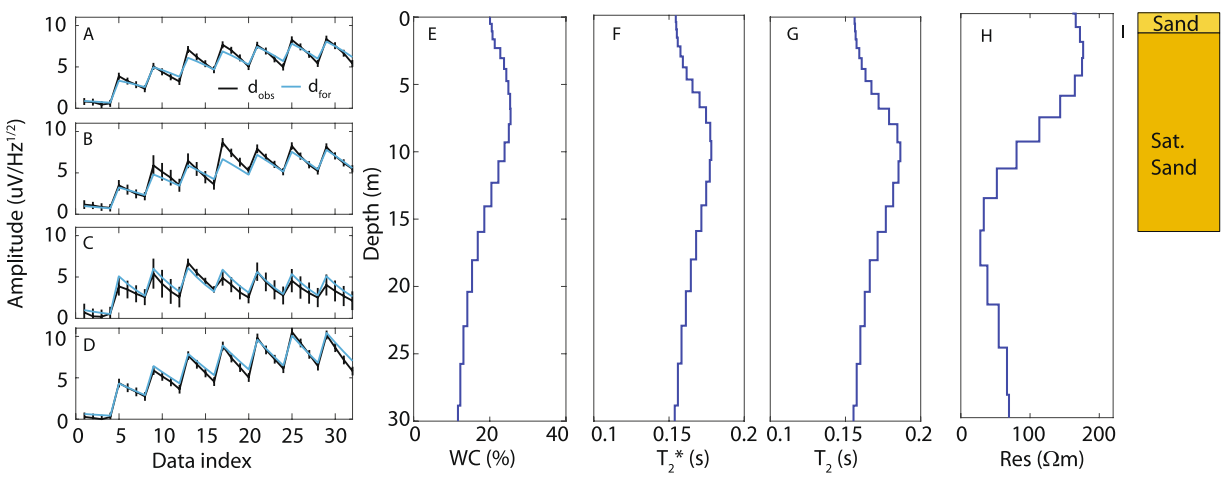

Figure 3. The data fit and profiles corresponding to data collected near Sunds, Denmark. (a–d) illustrate the observed and forward modeled data (black and blue, respectively), corresponding to the water content (e), T_2* (f), T_2 (g), resistivity (h), and lithology (i) profiles on the right.

the signal by a boxcar window with a period of $2t_{rep}$. In the case of a stationary powerline signal modeled as a unit-amplitude complex exponential, $e^{i\omega_n t}$, the contribution to the boxcar weighted DFT taken at ω_j is given by

$$S(\omega_j) = \int_0^{t_{max}} w(t) e^{i\omega_n t} e^{-i\omega_j t} dt \tag{7}$$

where $w(t)$ is the alternating boxcar window. The boxcar window can be cast as a sum of cosines,

$$w(t) = \sum_k A_k \cos\left(2\pi k t \left(\frac{2}{t_{rep}}\right)\right) = \sum_k \frac{A_k}{2}\left(e^{2\pi i k t\left(\frac{2}{t_{rep}}\right)} + e^{-2\pi i k t\left(\frac{2}{t_{rep}}\right)}\right) \tag{8}$$

Here, A_k is the coefficient describing the magnitude of the k'th component. Substituting Equation 8 into Equation 7 for the k'th component gives

$$\begin{aligned} S(\omega_j) &= \frac{1}{2}\int_0^{t_{max}} \left(e^{2\pi i k t\left(\frac{2}{t_{rep}}\right)} + e^{-2\pi i k t\left(\frac{2}{t_{rep}}\right)}\right) e^{i\omega_n t} e^{-i\omega_j t} dt \\ &= \frac{1}{2}\int_0^{t_{max}} e^{it\left(\omega_n + \frac{4\pi k}{t_{rep}}\right)} e^{-i\omega_j t} dt + \frac{1}{2}\int_0^{t_{max}} e^{it\left(\omega_n - \frac{4\pi k}{t_{rep}}\right)} e^{-i\omega_j t} dt \end{aligned} \tag{9}$$

Each of these integrals is maximized when

$$\omega_j = \omega_n \pm \frac{4\pi k}{t_{rep}}. \tag{10}$$

This shows that a stationary noise source oscillating at ω_n maximally contributes to the DFT taken at the frequencies given in Equation 10. The alternating behavior effectively modulates the powerline signal, shifting it into new locations in the frequency domain with the two closest being located at distances $2/t_{rep}$ Hz above and below its original location in the spectra. Very little energy from the ω_n noise source will appear in the DFT taken at $\omega_j = \omega_n$.

This feature can be exploited to separate an NMR signal from an overlapping co-frequency noise source. The alternating steady-state sequence preserves the location of the NMR signal in the spectra, while shifting troublesome noise sources a distance of $2/t_{rep}$ away. Figure 2d presents such an example. The NMR signal appears at 2,149.6 Hz, the estimated Larmor frequency, but no overlapping powerline harmonic is visible in this case. Instead, the powerline energy in the spectra has been moved approximately 5 Hz above and below its original location. Adequate separation between the NMR signal and the powerline harmonic is now present and a high quality signal is obtained, as seen in Figure 2h.

To demonstrate the ability to produce reliable models and satisfactory data fits using the frequency shifting approach, Figure 3 show the inversion results corresponding to the data in Figure 2 (Figures 3a–3d correspond to columns 1–4 in Figure 2). All four steady-state sequences are jointly inverted to form a single 1D-model of the water content, T_2*, and T_2. The overall data fit is $\chi^2 = 0.93$, indicating data is fit well within the estimated uncertainty levels. The inversion uses a surface NMR inversion based on a fast-mapping implementation (Grombacher, Kass, et al., 2020; Grombacher, Liu, et al., 2020) of a full-Bloch solution (Grombacher et al., 2019) for the surface NMR forward model. This is also observed in Figures 3a–3d where forward data (blue) generally falls within the error bars of the observed data (black). The data index corresponds to data collected for each sequence, with the decay for a single current amplitude measurement corresponding to a decay of four data points. Lower and higher data indices correspond to low and high amplitude currents, respectively. Note that the ability to simultaneously fit all four sequences highlights an ability to fit off-resonance and on-resonance simultaneously, as an on-resonance (alternating) sequence is fit using the same model as the three off-resonance (regular) sequences. The resulting depth profiles show a simple structure with an increase in water at shallow depths (~2 m), peaking at ~8 m, with a gradual transition to lower water contents below. The relaxation time profiles show a similar structure. This is consistent with nearby boreholes logs, which show a sand aquifer to at least ~15 m (bottom of the borehole). The water table is shallow in the area, observed to be ~1–2 m depth at nearby boreholes, consistent with the increase in water content at ~2 m Figure 3e. The T_2* and T_2 values are also consistent with that expected of sands—but have not been validated against an independent measure. The consistency between the T_2* and

T_2 profiles suggests a low magnetic susceptibility. The resistivity profile was collected using the tTEM system (Auken et al., 2019), and is used here only in the NMR kernel calculation. Overall, the resulting profiles agree very well with an expectation of a saturated sand unit, and produce satisfactory data fits for data that has been deliberately frequency shifted to avoid an overlapping powerline harmonic.

4. Discussion

The ability to shift the NMR signal or problematic noise sources to user-controlled locations in the spectra creates an opportunity to mitigate the impact of one of the most difficult noise sources in surface NMR; an overlapping narrow-band noise source. Traditional workflows based on demodulation and reconstruction of the NMR envelopes in the time-domain are unable to modify the relative frequency offsets between the NMR signal and troublesome noise sources. In these cases, one is forced to employ model-based removal approaches or remote reference approaches susceptible to overfitting or poor performance when the NMR and noise frequencies are too close or frequencies are varying fast, which may result in biased NMR signals. The proposed approach offers a greatly simplified solution in that it requires a minor (tens of microseconds) modification to repetition times, and the issue can be largely avoided without having to modify any subsequent processing workflows. Although no comparison to an FID acquisition is given in Figure 3, several studies have highlighted how troublesome overlapping powerline harmonics can be to FID data (Liu et al., 2017; Wang et al., 2018).

The ability to manipulate the location of the NMR signal in the spectra does not come for free. One must pay a projection efficiency penalty when deliberately shifting the signal off-resonance. The severity of the signal attenuation is illustrated in Figure 1c, where one can see that if the NMR signal is centered about 0 and a sequence is selected to project it some frequency away, its contribution to the DFT will be lower than if it were detected at its true frequency. However, in many circumstances it is advantageous for the signal-to-noise ratio to trade a small percentage of the signal amplitude in exchange for increased separation from a high-amplitude noise source. There are also limits on how far one can shift the NMR signal that arise from the comb-like behavior of the signal's spectra. Even when the steady-state signal is collected on-resonance, with the intention of producing a peak in the spectra at the Larmor frequency, there will still be shifted versions of the signal present at multiples of $2/t_{rep}$ away from the transmit frequency. As such, if one attempts to shift the signal a distance of $2/t_{rep}$, an identical spectrum will be produced (i.e., NMR signal's appearing at the same locations in the spectra) but with a penalty paid based on the $2/t_{rep}$ off-resonance excitation. As such, the effective maximum distance one can move the NMR signal is $1/t_{rep}$. This is the reason the data displayed in Figure 2 is collected with 5, 2.5, and 1.25 Hz offsets as these coincide with the maximum shifts for the ~100, ~200, and ~400 ms repetition times.

When employing regular steady-state sequences (i.e., identical polarity pulses) selecting the desired transmit frequencies and delay times can be done by maximizing the separation to known co-frequency noise source. For example, if one measures the Larmor frequency to be 2,149 Hz, one can select the maximum offsets that shift the NMR signal downwards in frequency away from the powerline harmonic that is likely present at 2,150 Hz. However, it is not always necessary to shift the signal if a narrow-band noise source is not close by in the spectra, as shifting the signal results in signal attenuation. For example, if one estimates the Larmor frequency to be 2,125 Hz (the midpoint between two powerline harmonics) there is no need to shift the signal. In this case, one should proceed with on-resonance workflows. Alternating sequences effectively employ an opposite strategy as regular sequences, in that they preserve the NMR signal location but shift noise sources to nearby locations in the frequency domain. One must be careful when employing alternating sequences nearby narrow-band noise sources so as to not shift the noise source on top of the NMR signal by accident. For example, if the sequence employed in the right-most column of Figure 2, which has a ~100 ms t_{rep}, is performed using a transmit frequency of 2,155 Hz, the 2,150 Hz powerline harmonic will be shifted 5 Hz up in the spectrum resulting in it now overlying the NMR signal. Therefore, a previously inconsequential noise-source may potentially destroy the signal if one is not careful. Although it may appear best to only employ alternating sequences, as the signal is left at its original location in the spectrum and projects most-efficiently, regular sequences remain useful given their differing sensitive volumes and relaxation time sensitivities compared to alternating sequences.

Another advantage of the proposed frequency shifting solution is that it can be readily automated to remove the need for a field operator to make the required adjustments on the fly. Instead, the estimated Larmor frequency can be used to define the suite of steady-state sequences that will be collected and a check can be automatically

performed to test whether the preliminary schemes are likely to overlap a narrow-band noise source (e.g., lie within ±2 Hz of a powerline harmonic) or if they are likely to shift a noise source onto the NMR signal for the alternating scenario. If overlapping noise sources are likely to be an issue, each sequence can be modified to maximize the separation.

The proposed approach effectively deals with the narrow-band noise sources during transmit, allowing minor modifications in acquisition to deal with these noise sources, in place of more complicated computationally expensive processing schemes. For example, the data presented in Figure 2 did not include any attempts to remove powerline noise from the signal, that is, no numerical powerline suppression techniques were employed. Despite this, high quality signals are produced in each case in one of the most difficult situations in surface NMR. The powerline in these cases has significantly more energy than the observed NMR signal, yet a simple DFT is capable of producing high-quality data. As such, these schemes are well-suited to field-processing workflows where near-real time feedback can be given to the operator to make assessments about data quality—for example, decide whether longer or shorter measurement intervals are necessary. Previously, in these scenarios one would be forced to collect data without being able to assess data quality in the field—as one typically does not have access to the computing power required of the model-based removal approaches.

The frequency shifting procedure involves deliberately transmitting off-resonance. As such, it is important that the offset between the detection (i.e., transmit frequency) and the estimated Larmor frequency be included in the forward modeling. Otherwise, the excitation modeling will not be done correctly, which can bias estimated water content and relaxation time curves in difficult to predict manners (Grombacher & Knight, 2015). Note that the repetition time is responsible for shifting the location of the NMR signal in the spectra, not the use of the DFT; for example, a spectra formed using a fast-Fourier transform displays the same signal shift.

5. Conclusions

Modifications to the repetition timing for surface NMR steady-state sequences allow the user to manipulate the location of the NMR signal in the spectrum. These minor timing changes can shift the signal away from problematic narrow-band noise sources such as powerline harmonics and provide significant mitigation of these noise sources without requiring computationally expensive model-based removal approaches. Alternating steady-state sequences are also shown to shift the location of relatively stationary noise sources away from their original locations in the spectra—thus allowing one to preserve the NMR signal location while moving problematic noise sources. The proposed workflow allows production of high-quality data in the presence of over-lapping noise sources, is easy to implement, and is well-suited to field data-processing and quality control. Overall, this approach vastly enhances the performance of surface NMR experiments under challenging co-frequency noise source scenarios.

Conflict of Interest

The authors declare no conflicts of interest relevant to this study.

Data Availability Statement

The data used to produce Figures 2 and 3 can be downloaded from https://doi.org/10.5281/zenodo.5764369.

Acknowledgments
This work is supported by funding from Independent Research Fund Denmark and VILLUM FONDEN (35816).

References

Auken, E., Foged, N., Larsen, J. J., Lassen, K. V. T., Maurya, P. K., Dath, S. M., & Eiskjær, T. T. (2019). tTEM—A towed transient electromagnetic system for detailed 3D imaging of the top 70 m of the subsurface. *Geophysics*, *84*(1), E13–E22. https://doi.org/10.1190/geo2018-0355.1

Carr, H. Y. (1958). Steady-state free precession in nuclear magnetic resonance. *Physical Review*, *112*(5), 1693–1701. https://doi.org/10.1103/PhysRev.112.1693

Grombacher, D., Fiandaca, G., & Auken, E. (2019). Estimating T2 from surface NMR FID data using a forward model based on the full-Bloch equation. *Geophysical Journal International*, *218*(3), 1892–1902. https://doi.org/10.1093/gji/ggz250

Grombacher, D., Kass, M. A., Auken, E., & Larsen, J. J. (2020). An approximate fast-mapping approach to the surface NMR forward problem. *Geophysical Journal International*, *221*(2), 928–937. https://doi.org/10.1093/gji/ggaa044

Grombacher, D., & Knight, R. (2015). The impact of off-resonance effects on water content estimates in surface nuclear magnetic resonance. *Geophysics*, *80*(6), E329–E342. https://doi.org/10.1190/geo2014-0402.1

Grombacher, D., Liu, L., Griffiths, M. P., Vang, M. Ø., & Larsen, J. J. (2021). *Steady-state surface NMR for mapping of groundwater*. Geophysical Research Letters. e2021GL095381. https://doi.org/10.1029/2021GL095381

Grombacher, D., Liu, L., Osterman, G. K., & Larsen, J. J. (2020). Mitigating narrowband noise sources close to the Larmor frequency in surface NMR. *IEEE Geoscience and Remote Sensing Letters*, *18*(8), 1376–1380. https://doi.org/10.1109/LGRS.2020.3000639

Grunewald, E., & Knight, R. (2011). The effect of pore size and magnetic susceptibility on the surface NMR relaxation parameter. *Near Surface Geophysics*, *9*(2), 169–178. https://doi.org/10.3997/1873-0604.2010062

Hertrich, M. (2008). Imaging of groundwater with nuclear magnetic resonance. *Progress in Nuclear Magnetic Resonance Spectroscopy*, *53*(4), 227–248. https://doi.org/10.1016/j.pnmrs.2008.01.002

Kenyon, W., Day, P., Straley, C., & Willemsen, J. (1988). A three-part study of NMR longitudinal relaxation properties of water saturated sandstones. *SPE Formation Evaluation*, *3*, 622–636. https://doi.org/10.2118/15643-pa

Larsen, J. J., Dalgaard, E., & Auken, E. (2014). Noise cancelling of MRS signals combining model based removal of powerline harmonics and multichannel Wiener filtering. *Geophysical Journal International*, *196*(2), 828–836. https://doi.org/10.1093/gji/ggt422

Larsen, J. J., Liu, L., Grombacher, D., Osterman, G., & Auken, E. (2020). Apsu—A new compact surface nuclear magnetic resonance system for groundwater investigation. *Geophysics*, *85*(2), JM1–JM11. https://doi.org/10.1190/geo2018-0779.1

Legchenko, A., & Valla, P. (2002). A review of the basic principles for proton magnetic resonance sounding measurements. *Journal of Applied Geophysics*, *50*(1–2), 3–19. https://doi.org/10.1016/s0926-9851(02)00127-1

Liu, L., Grombacher, D., Auken, E., & Larsen, J. J. (2017). Removal of co-frequency powerline harmonics from multichannel surface NMR data. *IEEE Geoscience and Remote Sensing Letters*, *15*(1), 53–57. https://doi.org/10.1109/LGRS.2017.2772790

Mohnke, O., & Yaramanci, U. (2008). Pore size distributions and hydraulic conductivities of rocks derived from magnetic resonance sounding relaxation data using multi-exponential decay time inversion. *Journal of Applied Geophysics*, *66*, 73–81. https://doi.org/10.1016/j.jappgeo.2008.05.002

Wang, Q., Jiang, C., & Müller-Petke, M. (2018). An alternative approach to handling co-frequency harmonics in surface nuclear magnetic resonance data. *Geophysical Journal International*, *215*(3), 1962–1973. https://doi.org/10.1093/gji/ggy389

Weichman, P. B., Lavely, E. M., & Ritzwoller, M. H. (2000). Theory of surface nuclear magnetic resonance with applications to geophysical imaging problems. *Physical Review E*, *62*, 1290–1312. https://doi.org/10.1103/PhysRevE.62.1290